ISSN 0016-7029, Geochemistry International, 2019, Vol. 57, No. 8, pp. 903–911. © Pleiades Publishing, Ltd., 2019.
Russian Text © The Author(s), 2019, published in Geokhimiya, 2019, No. 8.

Liquid Immiscibility in Regions of Localized Shock-Induced Melting in the Elga Meteorite

N. R. Khisina[a], *, R. Wirth[b], **, and A. M. Abdrakhimov[a], ***

[a] *Vernadsky Institute of Geochemistry and Analytical Chemistry of Russian Academy of Science, ul. Kosygina 19, Moscow, 119991 Russia*

[b] *GeoForschungZentrum Potsdam, Potsdam, 14473 Germany*

**e-mail: khisina@geokhi.ru,*

***e-mail: wirth@gfz-potsdam.de,*

****e-mail: AlbertAbd@gmail.com*

Received December 19, 2018; revised January 21, 2019; accepted February 12, 2019

Abstract—The regions of localized shock melting (melt pockets) in one of silicate inclusions in IIE Elga iron meteorite were investigated with EMPA, SEM, TEM and Raman spectroscopy. It has been established that the mechanism of formation of melt pockets in Elga is of a mixed nature, being associated not only with melting *in situ* of the silicate matrix, but also with the intrusion of portions of the melted schreibersite–oxide rim into the silicate inclusion. Melt pockets have an emulsion texture, which is a sign of phase separation by liquid immiscibility in high-temperature shock melts. The emulsion texture formed by droplet-shaped exsolutions of siderite in the schreibersite matrix of one of the melt pockets has all the features of phase separation by liquid immiscibility at superliquidus temperatures. This convincingly indicates the extraterrestrial origin of siderite in the Elga meteorite.

Keywords: IIE iron meteorites, melt pockets, shock melting, liquid immiscibility, meteorite Elga, siderite

DOI: 10.1134/S0016702919080068

INTRODUCTION

Collisions of cosmic bodies generate shock waves, which in turn, cause diverse shock effects in meteorites, in particular, deformation, brecciation, amorphization, as well as recrystallization with formation of new, including high-pressure, minerals (Stöffler et al., 1991; 2018; Sharp and DeCarli, 2006). As shock waves pass through material, they produce high pressures and temperatures reaching a few tens of GPa and a few thousands of degrees. The shock effects are maximized at boundaries between matters with different impedances[1]. This is accompanied by splitting the energy into diverse modes and a partial transformation of kinetic energy to heat, which is mainly accumulated in the lower density material (Kenkmann et al., 2000; Heider and Kenkmann, 2003). The presence of pore space (i.e., fractures and cavities) at the boundary of two diverse rocks intensifies shock effect, which results in the formation of localized melting zones such as impact veinlets and "melt pockets" (Kiefer, 1975; Kuchka et al., 2017; Walton and Spray, 2003; Walton and Show, 2009; Tomkins et al., 2013a; 2013b; Van Roosbroek et al., 2017).

Shock effects caused by the presence of a pore space at the boundaries of diverse matters are pronounced in the Elga meteorite, which is attributed to the IIE differentiated iron meteorite with silicate inclusions of several lithological types. It is generally accepted that Elga was formed by mixing of metallic and silicate melts at the surface of a parent body in response to a great impact event (Ruzicka, 2014). Mineralogy of silicate inclusions in Elga were described in (Kvasha et al., 1974; Plyashkevich, 1962; Osadchii et al., 1981; Teplyakova et al., 2018).

Peculiar effects caused by multiple shock events were revealed in the marginal parts of the Elga meteorite (Khisina et al., 2017a). The early shock event resulted in the formation of schreibersite-oxide reaction rims between a metal and a silicate, while the late event caused the formation of melt pockets in silicate inclusions, as well as partial fragmentation and brecciation of the rims. Siderite was identified among products of late impact event (Teplyakova et al., 2012; Khisina et al, 2017a; Senin et al., 2018). It is confined to the zones of shock transformation, being localized in an oxide layer of the rim, in a zone of rim brecciation, as well in phosphide–carbonate–oxide melt pocket within silicate inclusion.

In this work, melt pockets in polished thin section 2315.3.3A of the Elga meteorite were studied

[1] Impact resistance (impedance) is a shock wave velocity multiplied by the density.

using microprobe analysis, scanning electron microscopy, transmission electron microscopy, and Raman spectroscopy. Obtained results allowed us to propose a scenario of siderite formation through the impact transformation of the reaction rim.

LIQUID IMMISCIBILITY IN IMPACT MELTS

Melt pockets are zones of localized shock-induced melting observed in the different types of meteorites (Kuchka et al., 2017; Walton and Spray, 2003; Walton and Show, 2009; Tomkins et al., 2013a; Van Roosbroek et al., 2017). Their formation during impact event is provided by (1) extrusion of an impact melt from outside with filling fractures in rock or (2) in situ melting of rock surrounding the cavity or fracture owing to the closure of pore space.

The melt pockets frequently have emulsion texture, which is formed by phase separation through a liquid immiscibility (Van Roosbroek et al., 2017; Tomkins et al., 2013). The liquid immiscibility with formation of emulsion microtextures in oxide systems is well known in the glass and ceramics production (Mazurin and Porai-Koshits, 1984; Shelby, 2005; Shepilov et al., 2007) and was studied in the microspherules of industrial origin (Khisina and Wirth, 2011). Silicate–sulfide liquid immiscibility was discovered in the terrestrial volcanic rocks (Zolenski et al., 2018) and meteorites (Tomkins et al., 2013). Recent studies showed that the liquid immiscibility of silicate melts is widespread in a shock-transformed matter: in terrestrial impact rocks (Hamann et al., 2013; Hamann et al., 2018; Fazio et al., 2016), in meteorites (Van Roosbroek et al., 2017) and cosmic microspherules (Khisina et al., 2016). Emulsion textures formed by liquid immiscibility were experimentally modeled at normal pressure (Veksler et al., 2007), as well as obtained in shock experiments (Ebert et al., 2014; Hamann et al., 2018).

The liquid immiscibility field in the T–x phase diagram (x—composition) is bordered by binodal and spinodal curves, which characterize, respectively, the stable and metastable equilibrium in the system at superliquidus temperatures (Mazurin and Porai-Koshits, 1984; Shelby, 2005). The binodal and spinodal critical temperatures coincide; the spinodal curve is located within the region bordered by the binodal curve. Thermodynamics and mechanisms of phase separation by liquid immiscibility are described in detail in (Mazurin and Porai-Koshits, 1984; Shepilov et al., 2007; Shelby, 2005; Veksler et al., 2007). To produce the emulsion microtextures in the systems with liquid immiscibility, the following conditions should be met: (1) temperature of a melt formed by mixing of two and more melts must be higher than the binodal temperature for a given x composition in a system; (2) a melt should be homogenized and devoid of seeds (nucleii) of solid phase; (3) cooling rate of the melt should be sufficiently high to preserve emulsion textures. These conditions obviously could be fulfilled within melts of limited volume during shock-induced melting, with formation of localized melting zones, i.e., in melt pockets.

Phase separation caused by liquid immiscibility in a melt is easily identified from morphology of formed phases. The main morphological sign of the *binodal* unmixing is emulsion textures formed by globules, which are evenly of randomly distributed in a matrix. The chemical composition of the matrix differs from globule composition: globules are made up of component, whose content in the bulk melt was relatively low. Phase separation by *spinodal* decomposition occurs in melts, where immiscible components are present in nearly equal proportions. The spinodal decomposition leads to the formation of interconnected microtextures (Shepilov et al., 2007; Van Roosbroek et al., 2017; Mazurin and Porai-Koshits, 1984).

RESULTS AND DISCUSSION

Schreibersite–Oxide Rims

In the Elga meteorite, melt pockets are observed in mechanically weakened zone of silicate inclusions, being confined to cracks in silicate at the boundary with schreibersite–oxide rims. The schreibersite–oxide rims around silicate inclusions (Fig. 1a) are the characteristic feature of Elga. The elemental EDS/SEM mapping showed that the schreibersite–oxide rims are stratified: schreibersite $(Fe,Ni)_3P$ forms a layer at the contact with silicate, while oxide layer is located between the schreibersite and a host metal. The oxide layer of the rim is made up of Ni-bearing magnetite (Senin et al., 2017) and contains SiO_2 sublayer (Khisina et al., 2017b; Khisina et al., 2018). Schreibersite is cut by transverse cracks filled with a melt of FeO^{*}[2]–SiO_2–Al_2O_3 composition (Fig. 1b). This melt was obviously extruded from silicate inclusion through cracks in schreibersite to the contact with metal, where it formed the oxide layer. Troilite and siderite were identified in shock-metamorphosed zones of the schreibersite–oxide rim (Khisina et al., 2017a).

The stratified schreibersite–oxide rims are reaction zones formed at the metal–silicate boundary during the early shock event. Sources of phosphorus for the schreibersite layer were both silicate and FeNi metal (Osadchii et al., 1981; Khisina et al., 2018). After the passage of the shock wave, the contribution of phosphorus at the initial cooling stage was provided by dephosphorization of silicate matter (Osadchii et al., 1981). With further temperature decrease, incompatible P, S, and C were released from FeNi metal and supplied in melted reaction zone at the contact with the silicate inclusion (Khisina et al., 2018). The presence of troilite and siderite in the rim indicates a joint

[2] FeO* means that the valent state of iron in oxide was not determined.

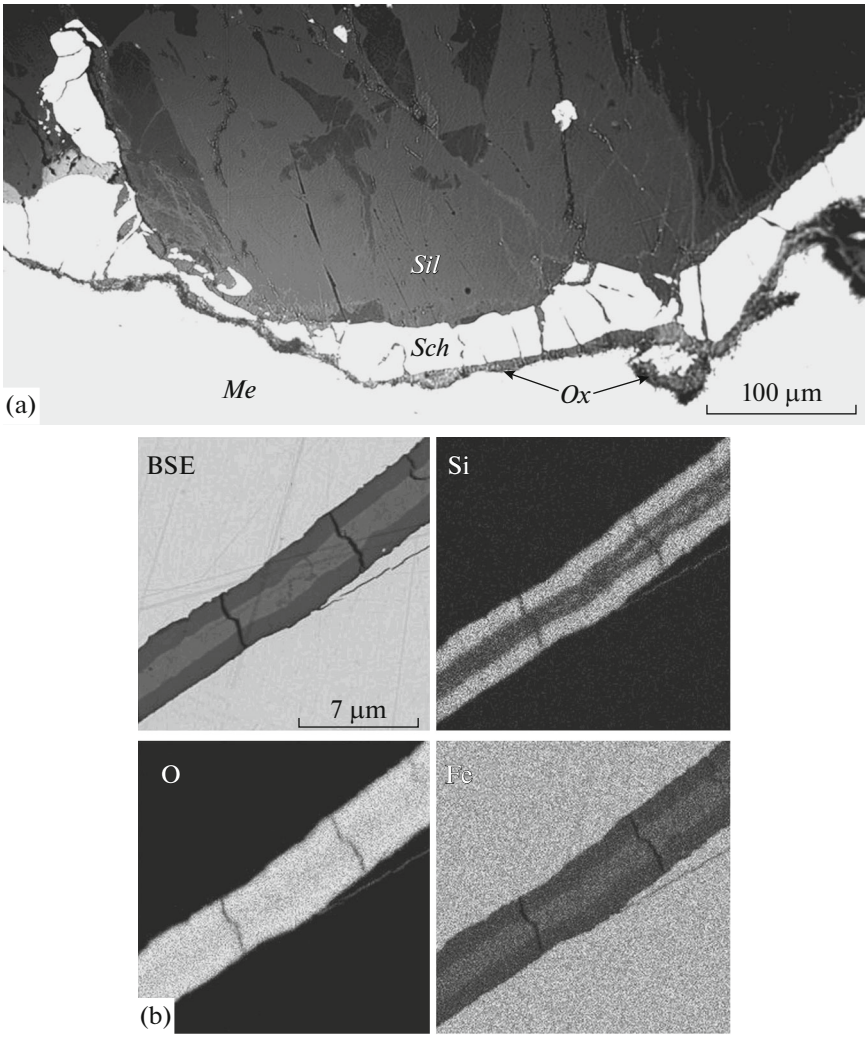

Fig. 1. (a) Schreibersite–oxide rim at the contact of a silicate inclusion and host metal in the Elga meteorite. Transverse cracks in schreibersite (gray) and layer between schreibersite and FeNi metal (gray) are filled with iron oxide and SiO_2. Optical image in a reflected light. (*Sch)* schreibersite, (*Me)* host metal, (*Ox)* oxide layer, (*Sil)* silicate inclusion. (b) Si, Fe, and O mapping of matter filling transverse cracks in schreibersite.

diffusion of incompatible S, C, and P in the schreibersite layer of the rim.

Melt Pockets

Melt pockets A, B, and C in Elga (Figs. 2, 3, 4) are restricted to cracks in a silicate inclusion and represent the products of shock-induced transformation of rim during late shock event. Melt pockets in Elga are formed by mixed mechanism, which involves melting *in situ* of silicate matrix adjacent to fractures and injection of portions of melted schreibersite–oxide rim into the silicate inclusion.

Melt pockets demonstrate emulsion microtexture typical of phase separation by liquid immiscibility in melts.

The emulsion texture is clearly expressed in the melt pocket A, which is confined to a crack in the silicate inclusion, which is connected with host FeNi metal (Fig. 2a). Numerous schreibersite globules are embedded in a silicate glass of the melt pocket, and the boundaries of the melt pocket are decorated by the finest globules. Emulsion texture indicates the formation of a homogenous shock-induced melt owing to the injection of melted phosphide fragment of the rim into the crack and its mixing with forming *in situ* silicate melt.

The boundaries of melt pocket B, which is also localized nearby the boundary between silicate inclusion and FeNi metal, are intensely decorated with small globules dispersed in a silicate glass (Fig. 2b). According to elemental EDS/SEM mapping, the silicate glass in the melt pocket has a pyroxene–feldspathic composition. The globules consist of alloys of schreibersite with FeNi metal and troilite (Fig. 3). Under the effect of shear deformation in a viscous

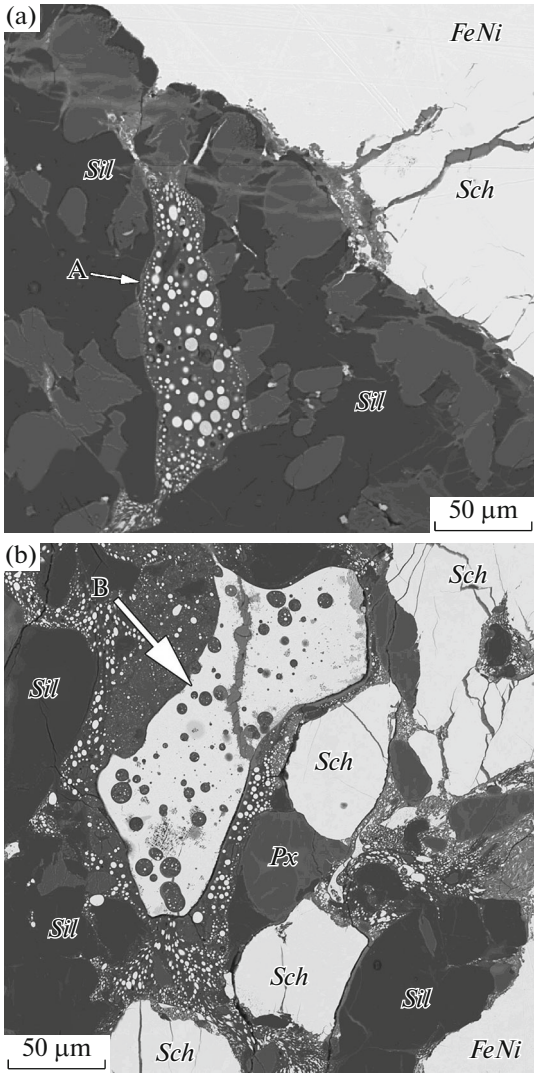

Fig. 2. Melt pockets A and B in a silicate inclusion. (a) Melt pocket A. Emulsion texture was formed during phase separation by binodal decomposition in a phosphide–silicate melt. (b) melt pocket B. Arrow shows FeNi–$(Fe,Ni)_3P$-FeS nodule with silicate globules. Emulsion texture in a silicate glass and in a nodule was formed owing to phase separation by binodal decomposition in a FeNi–$(Fe,Ni)_3P$–FeS–silicate melt. Nodules of pure schreibersite do not contain silicate globules. BSE image. (*Sch)* schreibersite, (Si*l)* silicate glass, (*Px)* pyroxene, (*FeNi)* host metal.

flow, the globules change their shape from spherical to ellipsoidal; this aspect is considered in (Tomkins et al., 2013a). In addition to numerous globules, the melt pocket B contains large nodule corresponding in composition to ternary alloy $(Fe,Ni)_3P$–FeS–FeNi (Figs. 2b, 3). The nodule contains large silicate globules, which, in turn, comprise very small nodules formed by a $(Fe,Ni)_3P$–FeS–FeNi alloy. This pattern corresponds to the secondary phase separation in metal–phosphide–sulfide melt. The emulsion textures in silicate glass and the nodules indicate a shock-induced melting with formation of mixed phosphide–sulfide–metal–silicate melt. This process was obviously accompanied by the extrusion of the schreibersite–troilite melt from the adjacent rim. At the same time, shock melting did not span the entire area shown in Fig. 2b. Closer to the silicate inclusion–metal boundary, the silicate contains "islands" devoid of the metal–schreibersite–troilite globules. Instead, the islands contain large nodules of pure schreibersite. The absence of silicate globules inside the schreibersite nodules indicates that schreibersite, unlike its alloys with troilite and metal, was not melted during shock-induced process. The schreibersite nodules were transferred from the adjacent schreibersite–oxide rim in a solid state and implanted in zones of unmelted silicate matter. Such conclusion is confirmed by preserved cracks in schreibersite, the absence of schreibersite globules in silicate glass at the contact with nodules, and the presence of unmelted pyroxene crystals in silicate melt.

Melt pocket C (Fig. 4) is located deep in a shock-transformed zone. This pocket (about 120 μm in size) is formed by a melted fragment of the schreibersite–oxide rim displaced deep in crack in the silicate inclusion. The melt pocket has a star-like shape, because the melt that formed it filled cracks diverging from the pocket boundary into silicate matrix. In addition to the main localization in melt pocket C, the shock-induced melt also formed small fragments dispersed in the surrounding silicate matrix. The boundary of melt pocket C is decorated by small schreibersite globules in a thin interlayer of silicate glass. In turn, the schreibersite matrix of melt pocket C contains silicate globules. The largest silicate globules contain nano-sized schreibersite globules, thus indicating secondary phase separation of silicate–phosphide melt in silicate globules by means of liquid immiscibility.

At optical magnifications, the melt pocket has a dendritic microtexture. However, TEM images revealed no dendritic morphology of precipitates. The precipitates in the schreibersite matrix have rounded shape, are isolated from each other, and evenly distributed. They are 1–2 μm in size and have spherical to ellipsoidal morphologies (Fig. 5). Melt pocket C frequently contains irregularly shaped segregations, which are enlarged by merging of globules and form "islands" with curved outlines in the schreibersite matrix (Fig. 6). Merging of globules (coalescence), like the secondary phase separation in globules, is caused by the evolution of emulsion texture during melt cooling (Hamann et al., 2013).

Previous studies discovered siderite in the melt pocket C (Teplyakova et al., 2012; Khisina et al., 2017a; 2017b; Senin et al., 2018). This caused a debate concerning the identification and origin of siderite in Elga. In this work, the identification of siderite was confirmed by electron diffraction and Raman spectroscopy. The Raman spectra of individual rounded

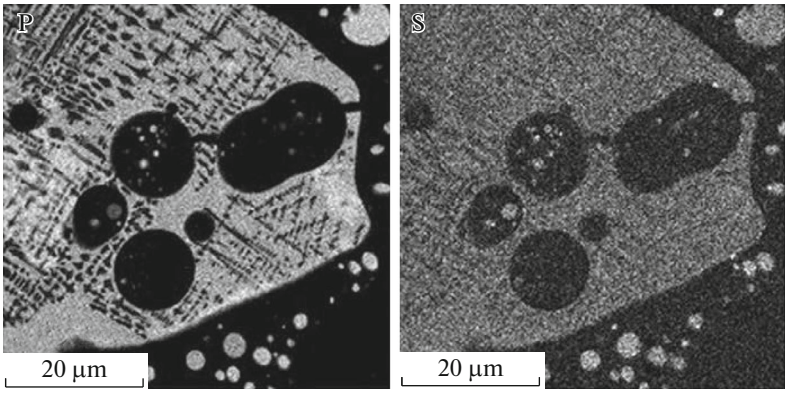

Fig. 3. Elemental mapping of phosphorus and sulfur distribution in a FeNi–$(Fe,Ni)_3P$–FeS nodule and adjacent glass. Melt pocket B.

grains embedded in a schreibersite matrix demonstrate a siderite band at 1082.6 cm^{-1} (Fig. 7a). The ring electron diffraction patterns of individual grains show diffuse reflections (Fig. 7b), which indicate that siderite exists as nano-crystalline aggregates. Measured interplanar spacings d_{hkl} (3.56, 2.75, 2.52, 2.314, 2.13, 1.768, 1.704, 1.497, 1.370 Å) correspond to siderite. Siderite inclusions in schreibersite are frequently surrounded by SiO_2 rim, which contains admixtures of Al, C, Fe; submicron inclusions of disordered carbon were identified in the rims. Siderite frequently contains domains with submicron Ni-phosphide (transjordanite?) and SiO_2 inclusions.

In addition to siderite, melt pocket C contains precipitates of iron phosphate (Fig. 8). The chemical composition of phosphate is determined as[3] 57.3 Fe, 0.9 Ca, 1.6 Mn, 0.2 K, 40.0 P (Senin et al., 2018), which is close to stoichiometry of sarcopside $Fe_3(PO_4)_2$. Matrix domains with sarcopside segregations are spatially separated from siderite-bearing domains. Domains with sarcopside segregations correspond to P-rich zones in the phosphorus distribution map of pocket C (Fig. 4b). Sarcopside segregations have an ellipsoidal shape and contain transverse cracks and cavities at the contact with schreibersite. Sarcopside grains contain silica-enriched regions with admixtures of K, Ca, and Mn. Segregations of nanosized Ni-phosphide (transjordanite?) are developed along the margins of the sarcopside grains.

In addition to the emulsion texture, the schreibersite matrix of melt pocket C comprises a 3D system of continuous worm-like precipitates about 150 nm in size (Figs. 6, 8). This texture is extended through the entire matrix, avoiding boundaries with sarcopside and siderite grains. The TEM–EDS spectra showed that the worm-like precipitates consisted of O, Si, C, Ni, and Fe with admixture of Ca, Al, and Mn. The Raman spectra and the TEM study revealed that the worm-like precipitates in melt pocket C contains Ni-bearing magnetite (Khisina et al., 2017a). The inter-

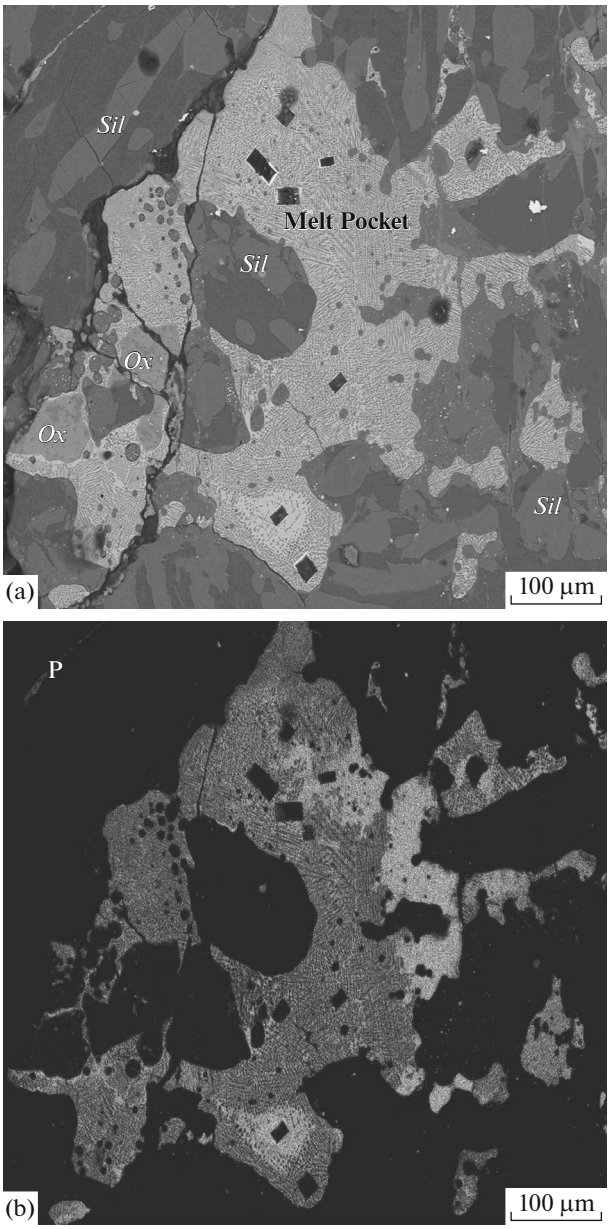

Fig. 4. Melt pocket C. (a) BSE/SEM image, (b) element mapping of phosphorus distribution.

[3] Element composition is given in at %.

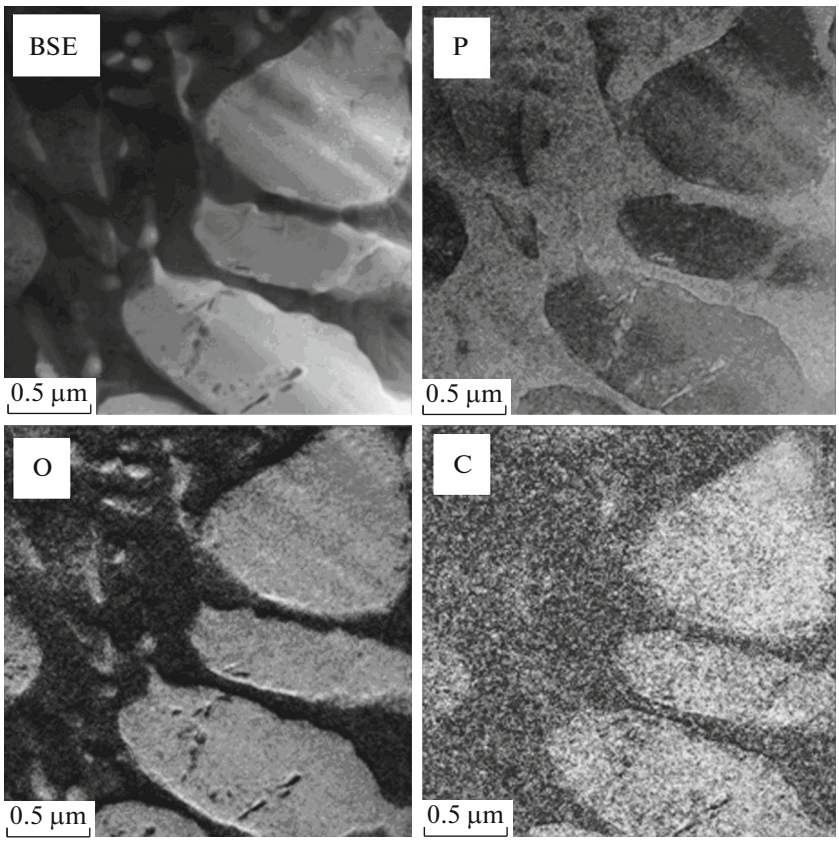

Fig. 5. Ellipsoidal siderite precipitates in a schreibersite matrix of melt pocket C. TEM image and corresponding EDS/TEM mapping of phosphorus, oxygen, and carbon distribution (Khisina et al., 2017a).

connected worm-like texture is indicative of the phase separation by spinodal decomposition (Mazurin and Porai-Koshits, 1984; Shelby, 2005).

Melt pockets B and C were produced during the same shock event. This late episode in the impact evolution of Elga led to melting of the schreibersite–oxide rim and injection of melted matter into the crack in a silicate inclusion. Migration of the melt along fractures was accompanied by the differentiation of matter by viscosity: the low-viscosity melt fractions migrate faster than melt fractions with higher viscosity (Tomkins et al., 2013). Correspondingly, the portions of the less viscous phosphide–oxide–carbonate melt migrated in cracks for a larger distance from the boundary with rim, with formation of melt pocket C. The more viscous phosphide–sulfide melt was accumulated near the boundary with rim and mixed with forming *in situ* silicate melt, thus generating pocket B.

Redox Reactions and Phase Separation in the Melt Pockets of Elga

Melt pocket C represents a phosphide–oxide–carbonate fraction of melt formed by shock-induced melting of the schreibersite–oxide rim. The rim contains schreibersite, $(Fe,Ni)_3P$, Ni-bearing magnetite, and SiO_2. Troilite and siderite were identified in shock-metamorphosed zones of the rim (Khisina et al., 2018). This implies that sulfur and carbon were initially incorporated in the schreibersite layer of the rim. Sulfur and carbon, in addition to phosphorus, are incompatible elements in the FeNi metal. We suggest that these elements diffused from the metal in the reaction zone at the contact with silicate and were involved in the schreibersite layer of the rim during its formation in the course of the early shock event (Khisina et al., 2018).

In shock process, melts are generated and homogenized at high temperatures, which result from the interaction of a shock wave with pore space in rock (Sharp and DeCarli, 2006). Subsequent phase separation by liquid immiscibility occurred during cooling of homogenized shock-induced melt. Homogenization temperature of multicomponent melt was higher than the binodal temperature and, respectively, higher than the liquidus temperature and, correspondingly, the melting temperatures of separate phases forming given melt. The melt formed by melting of a mixture of schreibersite, Ni-bearing magnetite, SiO_2, and carbon should be homogenized at higher temperature than the melting temperature of the most refractory phase–

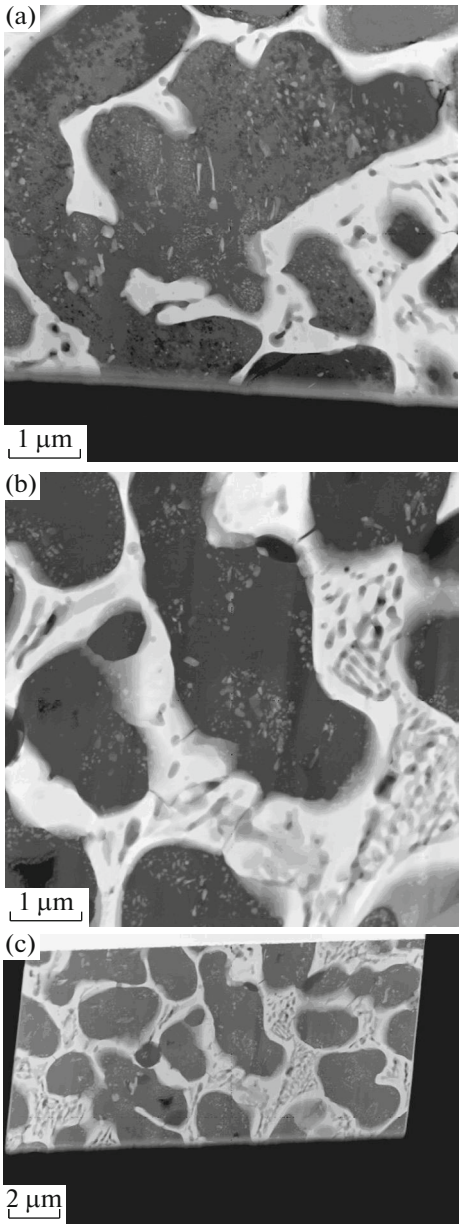

Fig. 6. Portions of melt inclusion C with large segregations of siderite (black) in a schreibersite matrix (light).

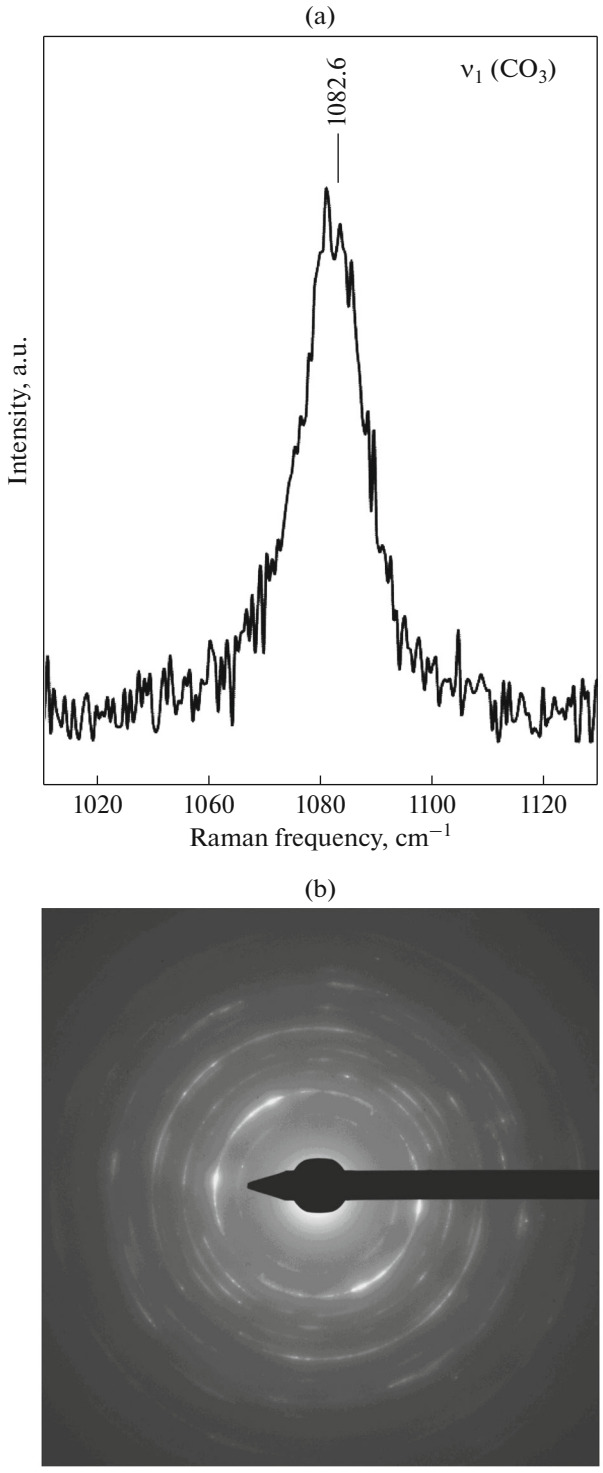

Fig. 7. Raman spectrum (a) and electron diffraction pattern (b) of individual siderite grain in a schreibersite matrix in melt pocket C.

SiO_2[4]. We suggest that the homogenization was accompanied by the self-reduction of Ni-bearing magnetite and formation of CO according to reactions $2NiO = 2Ni + O_2$, $2Fe_3O_4 = 6FeO + O_2$, and $2C + O_2 = 2CO$. During subsequent cooling, the melt was immiscibly split into phosphate and carbonate melts according to redox reactions: $2CO = C + CO_2$, $FeO + CO_2 = FeCO_3$, $3FeO + 1/2O_2 = Fe_3O_4$, $3FeO + 2P + 5/2O_2 = Fe_3(PO_4)_2$, $2Ni + P = Ni_2P$.

Based on obtained data, the texture of melt pocket C could be interpreted as result of subsequent stages of phase separation by liquid immiscibility in a cooling multicomponent melt.

(1) During post-shock cooling, homogenized and saturated by oxygen and CO_2 multicomponent

[4] Temperature of SiO_2 melting at normal pressure of 1710°C.

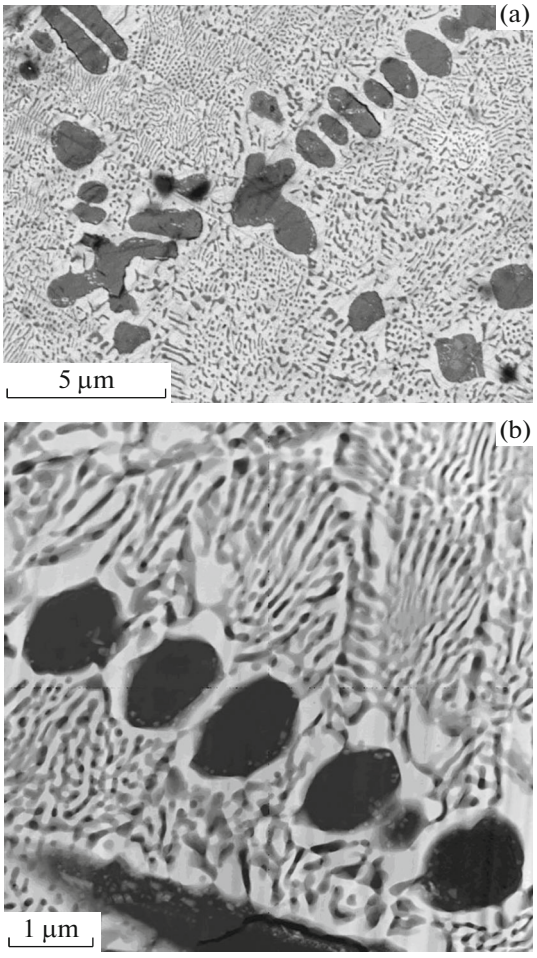

Fig. 8. Emulsion texture formed by ellipsoidal precioitates of sarcopside in P-rich portion of melt pocket C. Worm-like dark contrast in a schreibersite matrix is caused by phase separation following spinodal decomposition in a $(Fe,Ni)_3P$–FeO*–NiO–SiO_2–CO_2 melt. (a) BSE/SEM image; (b) TEM image.

$(Fe,Ni)_3P$–FeO–NiO–SiO_2 melt was exsolved into two immiscible melts: oxygen-rich and CO_2-rich. These melts were spatially separated from each other within melt pocket. With temperature decrease, phase separation in oxygen- and CO_2-rich regions were controlled by different mechanisms.

(2) CO_2-rich $(Fe,Ni)_3P$–FeO–SiO_2 melt was split with formation of SiO_2-doped $FeCO_3$ droplets in a melted SiO_2-doped $(Fe,Ni)_3P$, matrix. This process was driven by binodal decomposition. Siderite droplets coalesced to form rounded irregularly shaped globules in a schreibersite matrix.

(3) Oxygen-rich portions of melt pocket were characterized by the redistribution of elements and redox reactions between liquid phosphide phase and liquid iron oxide (Fe_3O_4) with formation of sarcopside in a schreibersite matrix.

(4) Further decrease of temperature led to secondary phase separation in the droplets of siderite, sarcopside, and in the schreibersite matrix, all of which contained admixtures of SiO_2, FeO*, and NiO. The secondary phase separation resulted in the formation of SiO_2 rims in siderite; segregation of submicron SiO_2 in siderite and sarcopside; and submicron Ni_2P (transjordanite?) in sarcopside. A continuous 3D system of worm-like precipitates containing SiO_2, FeO*, and NiO was formed in a schreibersite matrix. Worm-like texture in schreibersite is consistent with phase separation controlled by spinodal decomposition.

(5) Schreibersite crystallized before solidification of siderite and sarcopside. Crystallizing schreibersite matrix probably controled the observed arrangement of siderite and sarcopside in a melt pocket.

CONCLUSIONS

The emulsion texture of melt pockets in Elga indicates phase separation caused by liquid immiscibility, which occurred during cooling of shock-induced melt. Finding of siderite in a melt pocket C points to liquid immiscibility in oxygen- and CO_2–rich shock-induced multicomponent melt of $(Fe,Ni)_3P$–FeO–NiO–SiO_2 composition and convincingly supports the extraterrestrial origin of siderite in Elga.

Results of studies of melt pockets in Elga are consistent with inferred role of pore space in the formation of localized shock melting zones in meteorites. Obtained data demonstrate peculiarities of shock melting in the presence of pore space (cavities, microcracks) at the contact of phases with different impedances: (1) formation of mixed melt consisting of components of interacting matters with different impedances; (2) liquid immiscibility in forming melt pockets; (3) migration of unaltered fragments of denser matter (nodules) into less dense melted zones with formation of mixed ("solid–melt") melt pockets; (4) mobilization of volatiles and their accumulation in a pore space of shock melting zones; (5) self-oxidation–self-reduction in the shock melted zones owing to the dissociation of volatiles and fusible compounds.

ACKNOWLEDGMENTS

We are grateful to A. Burmistrov and E. A. Pankrushina for help in the performance of SEM and Raman spectroscopic studies. K. A. Lorenz is thanked for constructive review.

FUNDING

The work is partially supported by the Presidium of the Russian Academy of Sciences (program no. 28).

REFERENCES

M. Ebert, L. Hecht, A. Deutsch, T. Kenkmann, R. Wirth, and J. Berndt "Geochemical processes between steel projectiles and silica-rich targets in hypervelocity impact," Geochim. Cosmochim. Acta **133,** 257–279 (2014).

A. Fazio, M. D'Orazio, C. Cordie, and L. Folco, "Target-projectile interaction during impact melting at Kamil crater, Egypt," Geochim. Cosmochim. Acta **180,** 33–50 (2016).

C. Hamann, L. Hecht, M. Ebert, and R. Wirth, "Chemical projectile-target interaction and liquid immiscibility in impact glass from the Wabar craters, Saudi Arabia," Geochim. Cosmochim. Acta **121,** 291–310 (2013).

C. Hamann, A. Fazio, M. Ebert, L. Hecht, R. Wirth, L. Folco, A. Deutsch, and W. U. Reinold, "Silicate liquid immiscibility in impact melts," Meteorit. Planet. Sci. **53,** 1594–1632 (2018).

N. Heider and T. Kenkmann, "Numerical simulation of temperature effects at fissures due to shock loading," Meteorit. Planet. Sci. **38,** 1451–1460 (2003).

T. Kenkmann, U. Hornemann, and D. Stöffler, "Experimental generation of shock-induced pseudotachylites," Meteorit. Planet. Sci. **35,** 1275–1290 (2000).

N. R. Khisina and R. Wirth, "Chemical and phase heterogeneity of Ti–Fe–Mn–silica microspherules in crushed ore samples," Geochem. Int. **49** (11), 1111–1119 (2011).

N. R. Khisina, D. D. Badyukov, and R. Wirth, "Microstructure, nanomineralogy and local chemistry of cryptocrystalline cosmic spherules," Geochem. Int. **54** (1), 68–77 (2016).

N. R. Khisina, S. N. Teplyakova, R. Wirth, V. G. Senin, A. A. Averin, and A. A. Shiryaev, "Carbon-bearing phases in shock-induced melt zones of the Elga meteorite," Geochem. Int. **55** (4), 317–329 (2017a).

N. R. Khisina, A. A. Burmistrova, A. A. Shiryaev, A. A. Averin, V. G. Senin, and N. G. Zinov'eva, "Impact effects in the Elga iron meteorite with silicate inclusions (IIE group)," Proceedings of 18th International Conference "Physicochemical and Petrophysical Studies in the Earth's Science, (IGEM RAN, Moscow, 2017b), p. 284 [in Russian].

N. R. Khisina, R. Wirth, A. Burmistrov, A. A. Shiryaev, A. A. Averin, N. G. Zinovieva, E. Pankrushina, and A. M. Abdrakhimov, "Shock-produced siderite in IIE iron meteorite Elga: a secondary mineral of extraterrestrial origin," Meteorit. Planet. Sci. **53**(S1), 133 (2018).

S. W. Kiefer, "From regolith to rock by shock," The Moon **13,** 301–320 (1975).

C. R. Kuchka, C. D. K. Herd, E. L. Walton, Y. Guan, and Y. Liu, "Martian low-temperature alteration minerals in shock melt pockets in Tissint: constraints on their preservation in shergottite meteorites," Geochim. Cosmochim. Acta **210,** 228–246 (2017).

L. G. Kvasha, Yu. Terent'eva, and N. V. Sobolev, "Silicate inclusions and impact metamorphism in he Elga meteorite, Meteoritika **33,** 143–147 (1974).

O. V. Mazurin and E. A. Porai-Koshits, "The structure of phase-separated glasses," *Phase Separation in Glass,* Ed. by O. V. Mazurin and E. A. Porai-Koshits (Elsevier Science Publishing Company Inc., Amsterdam, 1984), pp. 163–200.

Eu. G. Osadchii, G. V. Baryshnikova, and G. V. Novikov, "The Elga meteorite: silicate inclusions and shock metamorphism," Proc. Lunar Planet. Sci. **12B,** 1049–1068 (1981).

L. N. Plyashkevich, "Some data on the composition and texture of the Elga iron meteorite," Meteoritika **22,** 51–60 (1962).

A. Ruzicka, "Silicate-bearing iron meteorites and their implications for the evolution of asteroidal parent bodies," Chem. Erde **74,** 3–48 (2014).

V. G. Senin, N. G. Zinov'eva, E. A. Pankrushina, A. A. Averin, and N. R. Khisina, "Identification of minerals in impact melting domains of the Elga meteorite," *Proceedings of All-Russian Annual Seminar on the Experimental Mineralogy, Petrology, and Geochemistry,* Ed. by O. A. Lukanin (GEOKHI RAS, Moscow, 2018), pp. 356–359.

T. G. Sharp and P. S. DeCarli, "Shock effects in meteorites," *Meteorites and the Early Solar System II*, Ed. by D. S. Lauretta and H. Y. McSween, (Univ. of Arizona Press, Tuscon, 2006), pp. 653–677.

J. E. Shelby, *Introduction to Glass Science and Technology, 2nd ed*. (Royal Society of Chemistry, Cambridge, 2005).

M. P. Shepilov, A. E. Kalmykov, and G. A. Sycheva, "Liquid–liquid phase separation in sodium borosilicate glass: ordering phenomena in particle arrangement," J. Non-Cryst. Solids **353,** 2415–2430 (2007).

D. Stöffler, K. Keil, and E. R. D. Scott, "Shock metamorphism of ordinary chondrites," Geochim. Cosmochim Acta **55** (12), 3845–3867 (1991).

D. Stöffler, C. Hamann, and K. Metzler, "Shock metamorphism of planetary silicate rocks and sediments: proposal for an updated classification," Meteorit. Planet. Sci. **53,** 5–49 (2018).

S. N. Teplyakova, K. A. Lorentz, M. A. Ivanova, N. N. Kononkova, M. O. Anosova, K. M. Ryazantzev, and Yu. A. Kostitzin, "Mineralogy of silicate inclusions in IIE iron meteorite Elga," Geochem. Int. **56**(1), 1–23 (2018).

S. N. Teplyakova, N. R. Khisina, and A. L. Vasil'ev, "Nanomineralogy of dendritic inclusion in the Elga iron meteorite," Zap. Ross. Mineral. O-va **141** (2), 42–52 (2012).

A. G. Tomkins, R. F. Weinberg, B. F. Schaefer, and A. Langendam, "Disequilibrium melting and melt migration driven by impacts: implications for rapid planetesimal core formation," Geochim. Cosmochim. Acta **100,** 41–59 (2013).

N. Van Roosbroek, C. Hamann, S. McKibbin, A. Greshake, R. Wirth, L. Pittarello, L. Hecht, P. Claeys, and V. Debaille, "Immiscible silicate liquids and phosphoran olivine in Netschaevo IIE silicate: analogue for planetesimal core-mantle boundaries," Geochim. Cosmochim. Acta **197,** 378–395 (2017).

I. V. Veksler, A. M. Dorfman, A. A. Borisov, R. Wirth, and D. B. Dingwell, "Liquid immiscibility and the evolution of basaltic magma," J. Petrol. **48,** 2187–2210 (2007).

E. L. Walton and C. S. J. Shaw, "Understanding the textures and origin of shock melt pockets in Martian meteorites from petrographic studies, comparisons with terrestrial mantle xenoliths, and experimental studies," Meteorit. Planet. Sci. **44,** 55–76 (2009).

E. L. Walton and J. G. Spray, "Mineralogy, microtexture, and composition of shock-induced melt pockets in the Los Angeles basaltic shergottite," Meteorit. Planet. Sci. **38,** 1865–1875 (2003).

M. Zolenski, V. S. Kamenetsky, J. A. Mavrogenes, A. A. Gurenko, and L. V. Danyushevsky, "Silicate–sulfide liquid immiscibility in modern arc basalt (Tolbachik volcano, Kamchatka): Part I. Occurrence and compositions of sulfide melts," Chem. Geol. **478**, 102–111 (2018).

Translated by M. Bogina